CROATICA CHEMICA ACTA CCACAA **72** (2–3) 311–326 (1999)

ISSN-0011-1643
CCA-2579 *Original Scientific Paper*

Evidence of Mechanical Alloying in Ball Milled ZrO_2–Y_2O_3 System Based on HRTEM Image Processing Analysis*

Anđelka Tonejc,[a,**] *Antun Tonejc,*[a] *George W. Farrants,*[b] *and Sven Hovmöller*[c]

[a] *Department of Physics, Faculty of Science, University of Zagreb, Bijenička c. 32, 10000 Zagreb, Croatia*

[b] *Calidris, Sollentuna, Sweden*

[c] *Department of Structural Chemistry, Stockholm University, Stockholm, Sweden*

Received October 8, 1998; revised January 25, 1999; accepted January 26, 1999

We investigated, using high resolution electron microscopy and image processing, the early stages of the mechanical alloying process of a mixture of zirconia and yttrium oxide powders. Molar fraction of yttrium oxide was 0.10. We focused our investigation on the grain boundary region and the region of overlapping layers of zirconia and yttria. Fourier filtering revealed, at the atomic level, one possible sequence of alloying, which occurred in the grain boundary and in the overlapping layers.

Key words: HRTEM, image processing, ceramics, mechanical alloying, ball milling.

INTRODUCTION

In recent years, zirconia and its solid solutions have attracted scientists and technologists because of their desirable physical, mechanical, optical and other properties. In pure zirconia, ZrO_2, phase transitions occur at high temperature and are martensitic. Monoclinic zirconia (m-ZrO_2) reversibly

---

* Dedicated to Professor Boris Kamenar on the occasion of his 70th birthday.

** Author to whom correspondence should be addressed. (E-mail: andjelka.tonejc@phy.hr)

transforms to tetragonal zirconia (t-ZrO_2) at 1150 °C, which reversibly transforms to cubic zirconia (c-ZrO_2) at 2370 °C. Large volume changes occur during these transitions, and the tetragonal or cubic phases cannot be quenched to room temperature. Pure zirconia is useless at high temperatures since it cracks.[1] Partially stabilized zirconia (PSZ), *i.e.* solid solutions of other oxides in zirconia, is generally recognized as the ceramic material having most useful mechanical properties, and thus named "ceramic steel".[2] Stabilization of the high temperature cubic phase at room temperature is possible by alloying zirconia with other oxides, such as MnO, NiO, Cr_2O_3, Fe_2O_3, Y_2O_3, Ce_2O_3. However, a very high temperature (over 1000 °C) of calcination or sintering is required for preparation of solid solutions of zirconia with these oxides.[3,4]

High energy ball-milling (mechanical alloying)[5,6] has become a widely used processing method for producing intermetallic compounds, extended solid solutions (even of immiscible elements), amorphous alloys and nanocrystalline materials.[7-9] However, high energy ball-milling (BM) was initially applied mainly to produce alloys formed from pure metals or intermetallic compounds, and it has been shown only recently[10] that mechanical alloying can also be used for ceramic materials (ZrO_2–Ce_2O_3 system).

Also, high energy ball-milling could be equivalent to thermal processes in achieving high temperature phase transitions.[11] Recently, it has been reported[12,13] that it is possible to synthesize cubic or tetragonal solid solutions of ZrO_2 with 16% (mass fraction) of Y_2O_3, CoO, Fe_2O_3 or α-Al_2O_3.

It is generally believed that alloying and amorphization are brought about by a solid state reaction during mechanical alloying as a mixture of thin layers.[14,15] This is the same mechanism as the one that occurs in thin films.[16] However, there is lack of transmission electron microscopy (TEM) and high resolution transmission electron microscopy (HRTEM) results in the literature to confirm this model of alloying process.[17,18]

The aim of the present work is to investigate the initial stages of the mechanical alloying process in m-$ZrO_2 + Y_2O_3$ ($x = 0.10$) powders using HRTEM image processing. We present the results obtained by applying the CRISP program[19] to analyze HRTEM photographs of mechanically alloyed materials.[20,21] The method described below could be applied in the investigation of other nanocrystalline materials.

EXPERIMENTAL

Powders of zirconia and yttria were milled for 10 minutes in a Fritsch planetary micro-ball mill Pulverisette 7, as reported previously.[11] The resulting specimens were examined using X-ray diffraction (XRD) by a PHILIPS PW 1820 diffractometer,

and using TEM (transmission electron microscopy) in a JEOL JEM 2010 electron microscope. This microscope has an accelerating voltage of 200 kV, a C_s of 0.5 mm and a point resolution of 0.19 nm. Powders were spread onto copper grids covered with holey carbon foil for TEM and HRTEM observations, and transparent regions were easily found.

RESULTS AND DISCUSSION

XRD, TEM and HRTEM Results

X-ray diffraction[13] and Raman spectroscopy[22] provided evidence of the formation of cubic zirconia solid solution. Figure 1 shows the change in XRD patterns of the powder mixture m-ZrO_2 + Y_2O_3 (x = 0.10) with the milling time. Although the mixture consisted of monoclinic zirconia (Figure 1a) and cubic Y_2O_3 (Figure 1b), the pattern of the mixture subjected to milling revealed that peaks of Y_2O_3 powder could still be seen and that the peaks of monoclinic zirconia broadened appreciably during the first 10 minutes of milling (Figure 1c). After 60 min of milling (Figure 1d), the peaks of Y_2O_3 were absent and the XRD pattern showed that about 54% of monoclinic phase was transformed into the tetragonal/cubic form. The fraction of tetra-

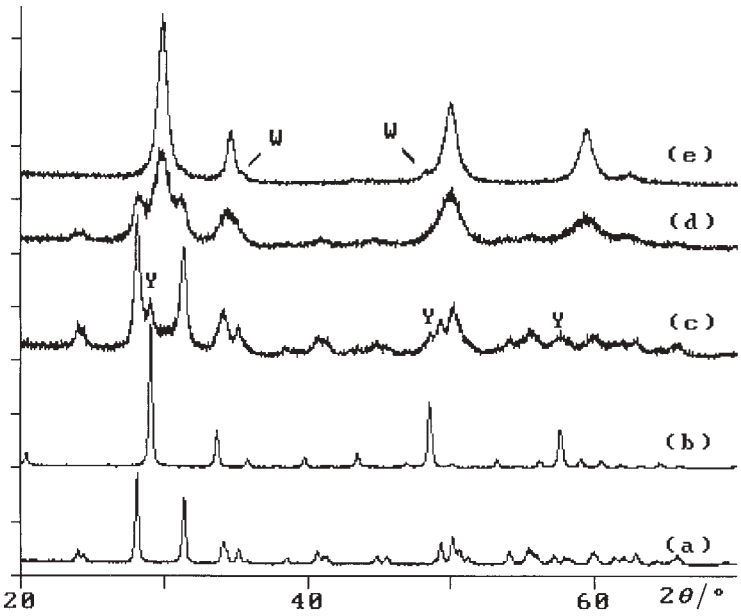

Figure 1. X-ray diffraction patterns of: (a) monoclinic ZrO_2; (b) cubic Y_2O_3; (c) mixture of m-ZrO_2 + Y_2O_3 (x = 0.10) milled for 10 minutes; (d) 60 min; (e) 180 min. Symbols: Y = Y_2O_3 ; W = WC.

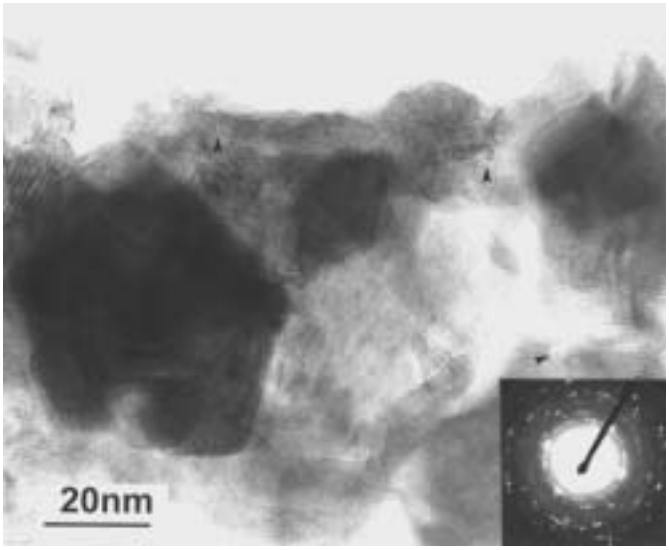

Figure 2. Variety of grain sizes in $ZrO_2 + Y_2O_3$ ($x = 0.10$) ball-milled for 10 minutes with the corresponding ED (in insert). Grain sizes of *m*-ZrO_2, *t*-ZrO_2 (5 nm grains, marked by arrow heads) and Y_2O_3, from 5 to 60 nm.

gonal cubic phase was estimated from the ratio of peak intensities: $(101)_T / [(\bar{1}11)_M + (101)_T + (111)_M]$.[23]

After 180 min of milling, only the cubic phase could be detected in XRD patterns[22] (Figure 1e). Very weak peaks, belonging to tungsten carbide (WC), could also be detected on XRD patterns, as a consequence of the wear of the balls and the vial.

Electron diffraction (ED), TEM and HRTEM experiments led us to the following observations:

i) Grains of *m*-ZrO_2, Y_2O_3 and *t*-ZrO_2 formed agglomerations (Figure 2). The presence of these types of grains was confirmed by electron diffraction, as shown in the insert. The grains have different sizes (from 5 to 60 nm) in different regions of the specimen.

ii) The grains of *m*-ZrO_2, Y_2O_3 and *t*-ZrO_2 contain internal faults, as shown in Figure 3. This figure otherwise confirms the grain agglomeration and grain size variety shown in Figure 2. The agglomeration of grains attached to a very large *m*-ZrO_2 grain is also of interest. Surface energy consideration indicated[23] that the grains smaller than 10 nm should be of tetragonal or cubic ZrO_2. However, our results show that defects are also important during the transition from monoclinic to tetragonal zirconia. The dark field image of the small grains A, B and C in Figure 3 was formed with

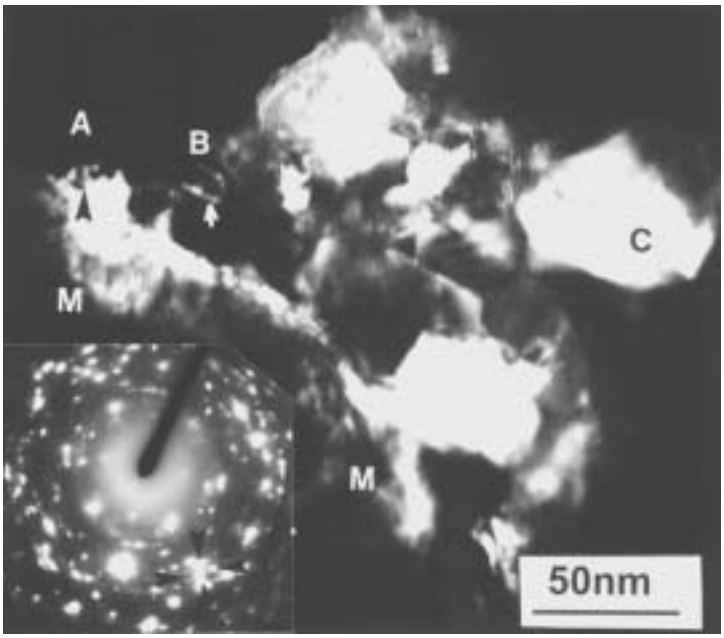

Figure 3. Dark field micrograph taken with the group of marked reflections from the corresponding ED pattern (in insert). Agglomeration of grains of m-ZrO_2 (M), t-ZrO_2 and Y_2O_3 (A,B,C). Some internal faulting is present in the grains.

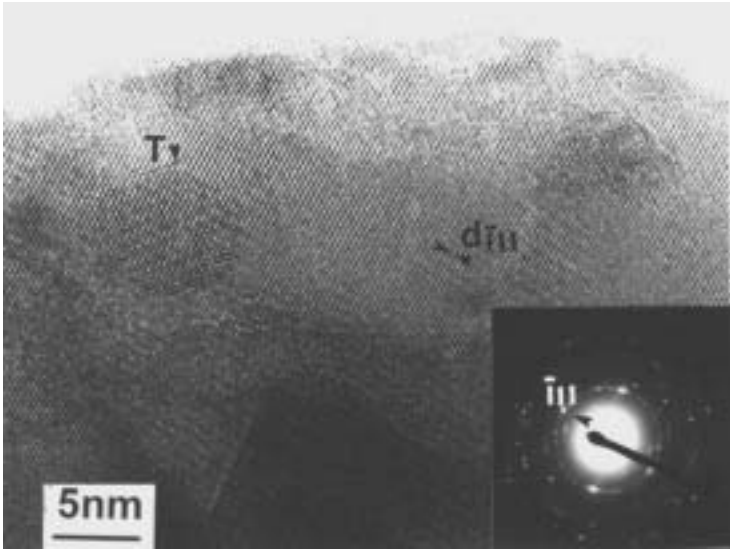

Figure 4. Nucleation of a small flake T of t-ZrO_2 on an m-ZrO_2 grain. The ($\bar{1}$11) lattice image, d = 0.316 nm. The corresponding ED pattern is given in the insert.

reflections of m-ZrO_2, t-ZrO_2 and Y_2O_3, as marked in the corresponding ED pattern (see the insert).

A layered structure induced by ball-milling is formed during the transition from monoclinic to tetragonal zirconia, where m-ZrO_2 grains slide relatively to each other and overlap (Figure 4). The $(\bar{1}11)$ lattice image (d = 0.316 nm) revealed shear deformation of lattice planes and plane rupture. Grains smaller than 10 nm are stuck onto a large grain as a thin layer of material (T). These small flakes of material have tetragonal nanocrystalline structure, as revealed in the corresponding ED pattern by diffraction rings, and they are the first grains of the new t-ZrO_2 phase. These grains are nucleated at m-ZrO_2 layers.

Image Processing of HRTEM Photographs

We obtained a further insight into the alloying process by image processing of HRTEM photographs. We will give one example from the early stages of the milling process. During milling, fragmentation and adhesion of the grains is a steady process. However, the newly formed interfaces between monoclinic zirconia grains and Y_2O_3 grains can be brought into intimate contact by subsequent ball collision forming a composite grain, as shown in Figure 5a. This is a HRTEM micrograph of a large monoclinic grain, M, almost in the $[\bar{1}0\bar{1}]$ orientation. From this region, we took two selected area diffraction photographs (SAD), shown in Figures 5b and 5c. In the SAD pattern, the strongest reflections belong to the m-ZrO_2 grain, M, and the weak reflections belong to the Y_2O_3 layer, L, in $[0\ \bar{1}\ \bar{1}]$ orientation. The region marked L is composed of m-ZrO_2 grain overlapped with the thin layer of Y_2O_3 in $[0\ \bar{1}\ \bar{1}]$ orientation. This is a direct evidence that alloying takes place in layers. Some other nanocrystalline Y_2O_3 grains distributed in the aggregate give additional spots, which form very sparse, spotty rings in the SAD pattern shown in Figure 5c.

The image processing analysis of this HRTEM image showed that further atomic mixing occurred in the grain boundary (GB) region as well as in the layers. Previously, it was also revealed,[17,18] using HRTEM and EDS (energy dispersive X-ray analysis), that layered structures are formed in ball-milled samples.

To elucidate the process of the solid-state reaction during ball-milling, we wanted to find out how Y_2O_3 penetrates into the m-ZrO_2 lattice and how this results in the formation of the tetragonal ZrO_2 solid solution (t-ZrO_2 SS). We calculated the diffraction pattern, *i.e.* the Fourier transform (FT), of the sample image. Each distinctive set of planes in the image will give a Fourier component in the calculated diffraction pattern, a bright spot (a "re-

flection") with a given amplitude and phase. Filtering of the spots in the diffraction pattern allows individual features in the original image to be reconstructed.

This method of filtering is a very general approach, and has been used in optical microscopy[24] and in electron microscopy.[25] In this approach, the crystal lattice of the specimen is considered as being built up of a number of gratings, each with its own spacing d. Image formation in the electron microscope proceeds by formation of a series of maxima in the back focal plane of the objective lens, each maximum having its own amplitude and phase. Recording this pattern would give the electron diffraction pattern, although phase information would be lost. However, if the electron beams then pass through the objective lens, they form the image.

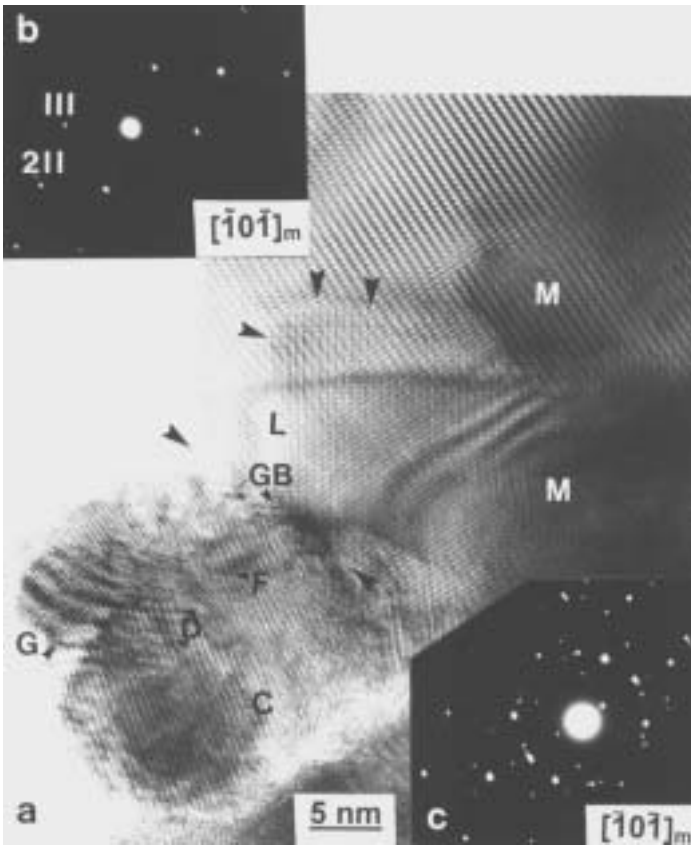

Figure 5. (a) HRTEM photograph of the mixture of m-ZrO_2 and Y_2O_3 powders ball-milled for 10 min; (b) ED pattern of (a) [$\bar{1}0\bar{1}$] m-ZrO_2; (c) ED pattern of (a) nearly [$\bar{1}0\bar{1}$] m-ZrO_2 ‖ [1 1 1] Y_2O_3 zone. The meaning of lettering is explained in the text.

The CRISP approach[26] to image processing is an inverse procedure. The calculated Fourier transform of the image corresponds to the ED pattern, with the important property that the phase information is preserved. Each of the gratings in the crystal lattice has given rise to a set of fringes in the image, and the calculated Fourier transform will contain one bright spot corresponding to each set of fringes. By selectively preserving information in the reflections, we can obtain information about the fringes in the image, and consequently also information about the structure of the crystal lattice. In particular, we can obtain information about a particular family of crystal planes.

The Fourier transforms of several regions in Figure 5a were calculated. The regions selected for study are marked in Figure 5a as:

– the grain boundary, GB;
– a region, L, of overlapping layers of zirconia and yttria;
– a region, F, containing stacking faults was analyzed in a previous work.[21]

The Results of Image Processing Analysis

The Fourier transforms (FT) of regions of size 256×256 pixels (corresponding to about 6×6 nm^2 in the specimen) were calculated. In each FT, masks with holes of radius 5 pixels were used to select components of the FT. The effect of the hole size was investigated within a range from 1 to 5 pixels, the largest size being chosen in order to ensure that very large reflections from the ZrO_2 were completely encircled by the mask hole. In Figure 6, two regions used for image processing are marked: the grain boundary region, GB, and the region of overlapping layers, L.

Grain Boundary Region

In the grain boundary region, we expect that the planes from the two adjacent grains form this grain boundary. The Fourier transform of the grain boundary region is shown in Figure 7j and shows that the projection is close to the $[\bar{1}0\bar{1}]$ zone of *m*-ZrO_2. This agrees with the ED pattern shown in Figures 5b and 5c. The reflections in the FT are marked by numbers 1 to 7, and are assigned to *m*-ZrO_2 and Y_2O_3, as shown in Table I. The reflection marked 7 was a complex spot containing three identifiable components, 7_1, 7_2 and 7_3, having slightly different *d*-values.

The results obtained after filtering using particular reflections are displayed in Figures 7a to 7l. Figure 7a shows the (111) lattice image of *m*-ZrO_2, which is obtained using reflection 1. Dislocations and deformations of the planes are revealed. Similarly, Figure 7b shows the (001) lattice image of *m*-ZrO_2, which is obtained using reflection 2, and Figure 7c shows the (211) lattice image of *m*-ZrO_2 from reflection 3.

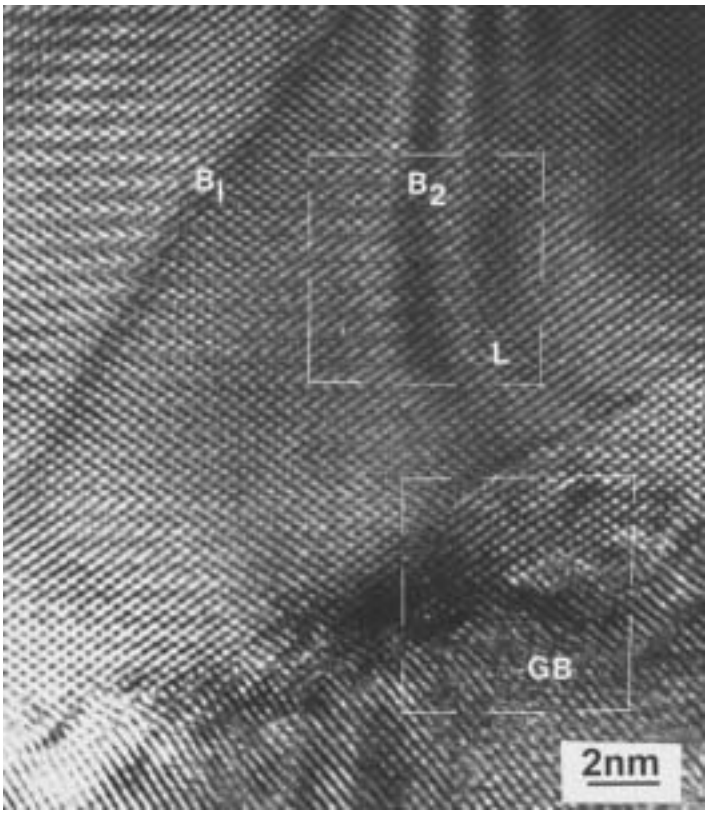

Figure 6. Grain boundary region GB and region of overlapping layers L. The areas used for image processing are marked.

TABLE I

d-Values assignment obtained from FT (Figure 7(j)) of the grain boundary region

Spot in FT	*d* / nm (measured)	*h, k, l* (calcd.)	Phase identified	*d* / nm (from lit.)	Corresponding lattice image
1	0.277–0.289	111	*m*-ZrO_2	0.284	Figure 7(a)
2	0.51	001	*m*-ZrO_2	0.508	Figure 7(b)
3	0.196	211	*m*-ZrO_2	0.202	Figure 7(c)
4	0.434	$\bar{2}11$	Y_2O_3	0.434	Figure 7(e)
5	0.434	211	Y_2O_3	0.434	Figure 7(d)
6	0.319–0.332	$\bar{1}11$	*m*-ZrO_2	0.316	Figure 7(g)
7_1	0.3164	$\bar{1}11$	*m*-ZrO_2	0.316	Figure 7(h)
7_2	0.285	111	*m*-ZrO_2	0.284	
7_3	0.306	222	Y_2O_3	0.306	

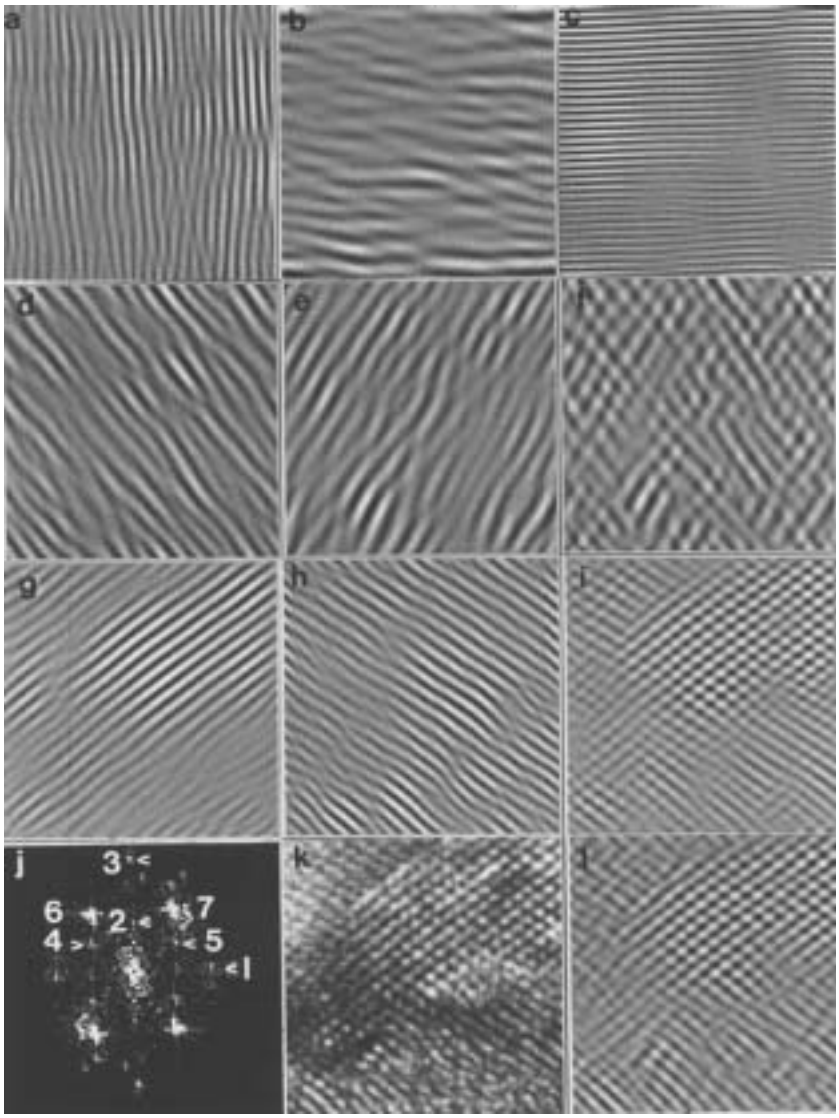

Figure 7. Filtered lattice images from grain boundary GB region obtained with particular diffraction spots from FT of Figure 7(j): (a) 1 – (111)*m*-ZrO_2, d = 0.284 nm; (b) 2 – (001)*m*-ZrO_2, d = 0.508 nm; (c) 3 – (211)*m*-ZrO_2, d = 0.202 nm; (d) 5 – (211)Y_20_3, d = 0.434 nm; (e) 4 – ($\bar{2}$11)Y_20_3, d = 0.434 nm; (f) superposition of (211) and ($\bar{2}$11) Y_2O_3 lattice images from (d) and (e); (g) 6 – ($\bar{1}$11)*m*-ZrO_2, d = 0.316 nm; (h) 7_1, 7_2, 7_3 – ($\bar{1}$11)*m*-ZrO_2, d = 0.316 nm, (111)*m*-ZrO_2, d = 0.284 nm and (222) Y_2O_3, d = 0.306 nm; (h) 6 – ($\bar{1}\bar{1}$1)m-ZrO_2, d = 0.316 nm; (i) superposition of lattice images of the main *m*-ZrO_2 reflections 6 and 7, from (g) and (h); (j) FT of the GB region; (k) reconstructed original image with all reflections from FT (j); (l) reconstructed image with superposition of (f) and (i) images.

Two symmetry related sets of planes from Y_2O_3 are shown in Figures 7d and 7e, corresponding to reflections 5 and 4. These two reflections are combined in the reconstruction shown in Figure 7f in order to reveal the appearance of yttria in the grain boundary region.

Figure 7g shows ($\bar{1}11$) lattice planes of ZrO_2 reconstructed from reflection 6, while Figure 7h shows the reconstruction obtained from reflections 7. As mentioned previously, the complex spot 7 contains contributions from three sets of planes, one of which is a ($\bar{1}11$) reflection related by symmetry to reflection 6. The reconstruction using both reflection 6 and reflections 7 is shown in Figure 7i, showing the reconstruction with one reflection from yttria (7_3) and three from zirconia (6, 7_1, 7_2). Figure 7l shows the reconstructed image with superposition of Figures 7f and 7i images, *i.e.* reconstruction using reflections (4, 5, 7_3) of yttria and reflections (6, 7_1, 7_2) from zirconia. Finally, Figure 7k shows the reconstruction using all the reflections in the FT.

Overlapping Layers L of Zirconia and Yttria

The electron diffraction pattern shown in Figure 5b and 5c is close to the [$\bar{1}0\bar{1}$] zone of *m*-ZrO_2 lattice. The faint reflections are due to Y_2O_3. It is not obvious whether the large grain M has a thin layer of Y_2O_3 overlapping it. Furthermore, we wanted to explain why the different regions of grain M have different appearances by determining the constituents of the HRTEM pattern. As grain M is bent, the bent contours B_1 and B_2 are observed (Figure 6). We performed the Fourier transform of different parts with masks having sizes 256×256 pixels and 512×512 pixels. All Fourier transforms

TABLE II

d-Values assignment obtained from FT (Figure 8(j)) of the region of layer L

Spot in FT	*d* / nm (measured)	*h, k, l* (calcd.)	Phase identified	*d* / nm (from lit.)	Corresponding lattice image
1	0.19	440	Y_2O_3	0.187	Figure 8(a)
		400	Y_2O_3	0.265	
2	0.265–0.247	200	*m*-ZrO_2	0.262	Figure 8(b)
3	0.256–0.246	400	Y_2O_3	0.265	Figure 8(c)
4	0.426	$\bar{2}11$	Y_2O_3	0.434	Figure 8(d)
5	0.435	211	Y_2O_3	0.434	Figure 8(e)
6	0.315	$\bar{1}11$	*m*-ZrO_2	0.316	Figure 8(h)
7_1	0.302–0.299	$\bar{1}11$	*m*-ZrO_2	0.316	
7_2	0.299	222	Y_2O_3	0.306	Figure 8(g)
7_3	0.323	$\bar{1}11$	*m*-ZrO_2	0.316	

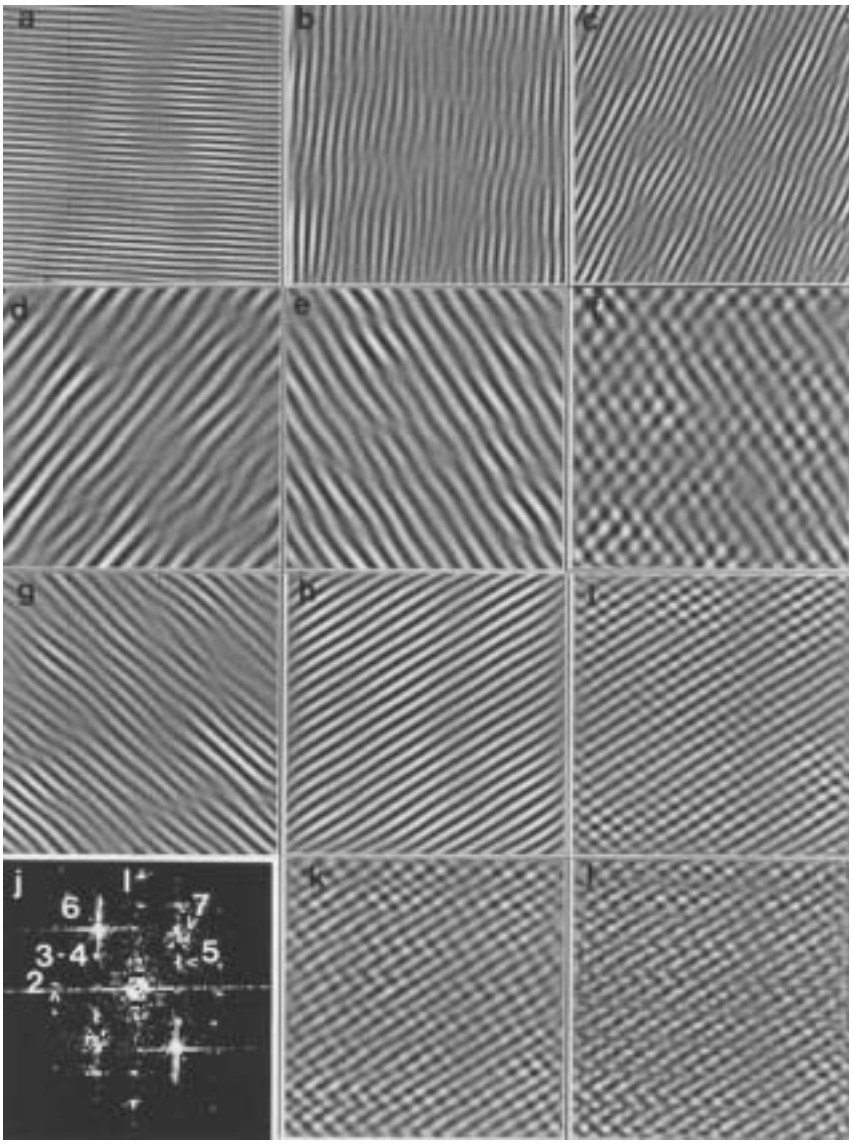

Figure 8. Filtered lattice images of the overlapping layers L obtained with particular diffraction spots from FT of Figure 8(j): (a) 1 – (440)Y_2O_3, d = 0.187 nm; (b) 2 – (200)m-ZrO_2, d = 0.262 nm; (c) 3 – (400)Y_2O_3, d = 0.265 nm; (d) 4 – $(\bar{2}11)Y_2O_3$, d = 0.434 nm; (e) 5 – (211)Y_2O_3, d = 0.434 nm; (f) superposition of images of yttria from (d) and (e); (g) 7_1, 7_2, 7_3 – $(\bar{1}11)m$-ZrO_2 , d = 0.316 nm, (222)Y_2O_3, d = 0.306 nm, $(\bar{1}11)m$-ZrO_2, d = 0,316 nm; (h) 6 – $(1\bar{1}1)m$-ZrO_2, d = 0.316 nm; (i) the superposition of lattice images of m-ZrO_2 6 and 7 from (g) and (h): (j) FT of the region L; (k) reconstructed image with superposition of (f) and (i) images; (l) reconstructed original image with all reflections from FT (j).

from this region had the same appearance (Figure 8j), indicating that the two zones, one from yttria and one from zirconia, are parallel, and that the layers are parallel. Reflections in the FT are marked by numbers from 1 to 7, and are assigned to m-ZrO_2 and Y_2O_3, as shown in Table II.

The results obtained after filtering, using particular reflections from FT of Figure 8j, are displayed in Figures 8a to 8l.

Figure 8a shows the (440) lattice image of Y_2O_3, which is obtained using reflection 1. Similarly, Figure 8b shows the (200) lattice image of m-ZrO_2, which is obtained using reflection 2, although the identification of this reflection is uncertain, and an alternative explanation could be (400) from Y_2O_3.

Figure 8c shows the (400) lattice image of Y_2O_3 from reflection 3. Two symmetry related sets of planes from Y_2O_3 are shown in Figures 8d and 8e, corresponding to reflections 4 and 5. These two reflections are combined in the reconstruction shown in Figure 8f.

Figure 8h shows the reconstruction from reflection 6, the $(\bar{1}11)$ from m-ZrO_2, while Figure 8g shows the reconstruction obtained from three reflections 7. The reconstruction using both reflection 6 and reflections 7 is shown in Figure 8i.

Figure 8k shows the reconstruction obtained when using contributions both from yttria and from m-ZrO_2, reflections 4, 5, 6 and 7_1, 7_2, 7_3. Finally, Figure 8l shows the reconstruction obtained with all the reflections identified in the FT (Figure 8j). We can see that this image reveals stripped details from the original HRTEM photograph of Figure 6 in the region marked L.

Figure 8l shows a periodicity of 0.74 nm, arising from the superposition of yttria and zirconia reflections. The Fourier transform and the ED pattern of this region have shown the strong streaked reflection from the $[\bar{1}0\bar{1}]$ zone of m-ZrO_2, while the faint reflections come from the $[01\bar{1}]$ zone of Y_2O_3 (see Figure 5c). This zone is parallel to the $(\bar{1}0\bar{1})$ of m-ZrO_2 (see Figure 5c, which means that the layers of zirconia and yttria are also parallel).

Refinement of Filtering Analysis

Spot 7 in the Fourier transform (FT) shown in Figure 8j is a multiple spot consisting of three components, and the reconstruction shown in Figure 8g is obtained when all three components are used.

Figure 9 shows filtered images obtained using mask holes, which allow different components of reflection 7 to contribute. Figure 9a shows the reconstruction obtained with a hole of radius one pixel, which isolates the $(\bar{1}11)$ planes of the m-ZrO_2 lattice. The lattice planes of m-ZrO_2 appear perfect without any distortion. A hole of size three pixels was used to obtain the reconstruction shown in Figure 9b, allowing all three components of reflection 7 to contribute.

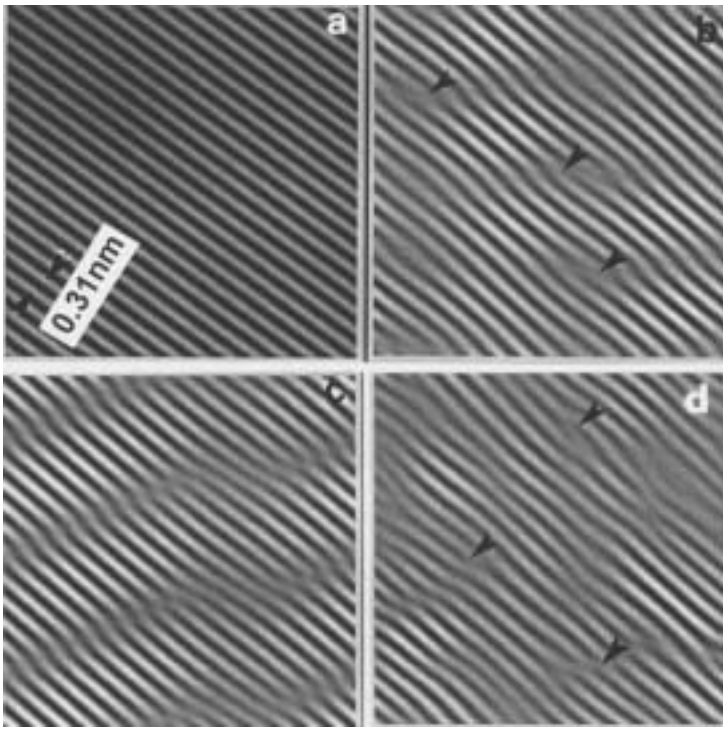

Figure 9. Refinement in overlapping layers L. Filtered lattice images with spots 7 (7_1,7_2,7_3): ($\bar{1}11$) *m*-ZrO_2, (222) Y_2O_3 , ($\bar{1}11$) *m*-ZrO_2 from FT of Figure 8(j) with different filtering mask radii: (a) ($\bar{1}11$) *m*-ZrO_2 (*d* = 0.316 nm), one pixel; (b) all spots 7, three pixel; (c) two spots 7_1 and 7_2, isolated with one pixel mask; (d) five pixels encircling all three spots 7.

Two components of reflections 7, 7_1 and 7_2, were allowed to contribute to the reconstruction shown in Figure 9c, using two separate holes, each of radius one pixel, while Figure 9d shows the reconstruction obtained with a hole of radius 5 pixels.

Image processing, in particular the use of Fourier filtering, has given a new insight into the fine details of HRTEM images, allowing us to draw conclusions about the physical processes occurring in the initial stages of mechanical alloying induced by ball-milling. Figures 9a to 9d provide information about the rupturing of the ($\bar{1}11$) *m*-ZrO_2 planes, *i.e.* about insertion of other ($\bar{1}11$) planes of ZrO_2 and penetration of (222) planes of Y_2O_3 into ($\bar{1}11$) *m*-ZrO_2 planes.

The images shown in Figures 9a to 9d allow the following physical interpretation. The rupture of planes in ball-milled samples occurs initially at the

level of 2.5 to 3 nm, shown by arrows in Figures 9b to 9d. We can identify intercalated planes having origin in other *m*-ZrO_2 and Y_2O_3 grains. These planes, indexed according to the corresponding FT, break into the perfect order of the $(\bar{1}11)$ monoclinic ZrO_2 lattice planes observed in Figure 9a.

CONCLUSIONS

We have reported here our results on the initial stages of the mechanical alloying process in ZrO_2–Y_2O_3 using an image processing analysis of HRTEM photograph. We draw the following conclusions:

- Image processing is a sensitive and precise method for analyzing grain boundaries and defects, including stacking faults and overlapping layers.
- Alloying of monoclinic zirconia and yttria and the formation of a new tetragonal ZrO_2 solid solution occur simultaneously.
- Nucleation of the new tetragonal ZrO_2 solid solution occurs in the form of small layers having 10 nm in diameter.
- Decrease of grain sizes is accompanied by stresses in the ball-milling procedure when the defects or stacking faults are formed. This conclusion is supported by the results of the Fourier filtering analysis where inserted planes and broken planes are observed (Figures 9c and 9d). These intercalated planes are assigned to particular planes according to the corresponding FT of the region.
- In the grain boundary region, we reveal the beginning of the alloying process as the inter-penetration of Y_2O_3 and *m*-ZrO_2 planes (Figure 7h and Table I). Some $(\bar{1}11)$ *m*-ZrO_2 planes traverse the grain boundary (Figure 7a), while others are broken. The broken planes form stacking faults, which accommodate the newly formed interface between grains.
- The refinement of Fourier filtering offers a new insight into the fine details of HRTEM images, allowing us to draw conclusions about the physical processes occurring in the initial stages of mechanical alloying induced by ball-milling. The rupture of planes in ball-milled samples occurs initially at the level of 2 to 3 nm (Figures 9b and 9d).

Acknowledgements. – The authors would like to thank dr. M. Stubičar for performing the ball-milling. We also want to thank the Croatian Ministry of Science and Technology for financial support (Project 119202).

REFERENCES

1. E. C. Subbaro, H. S. Maiti, and K. K. Srivastava, *Phys. Stat. Sol. (a)* **21** (1974) 9–15.
2. R. C. Garvie, R. H. Hannink, and R. T. Pascoe, *Nature* **258** (1975) 703–704.
3. A. Keshavaraja and A. V. Ramaswamy, *J. Mater. Res*. **9** (1994) 837–840.

4. M. C. Caracoche, P. C. Rivas, A. P. Pasquevich, and A. R. Lopez Garcia, *J. Mater. Res.* **8** (1993) 605–610.
5. J. S. Benjamin, *Metall. Trans.* **1** (1970) 2943–2951.
6. W. Weeber and H. Bakker, *Physica B* **153** (1988) 93–135.
7. C. C. Koch, *Mater. Sci. Forum* **88–90** (1992) 243–262.
8. P. H. Shingu (Ed.), *Mechanical Alloying*, Trans. Tech. Publications Ltd, Zürich, 1992.
9. R. Schulz (Ed.), *Metastable, Mechanically Alloyed and Nanocrystalline Materials,* Trans. Tech. Publications Ltd, Zürich, 1995.
10. Y. L. Chen and D. Z. Yang, *Scr. Metall.* **29** (1993) 1349–1351.
11. A. Tonejc, A. M. Tonejc, and D. Dužević, *Scr. Metall. Mater.* **25** (1991) 1111– 1113.
12. Y. L. Chen, M. Zhu, M. Qi, D. Z. Yang, and H. J. Fecht, *Mater. Sci. Forum* **179–181** (1995) 133–138.
13. A. M. Tonejc and A. Tonejc, *Mater. Sci. Forum* **225–227** (1996) 497–502.
14. P. J. Desré and A. R. Yavary, *Phys. Rev. Lett.* **65** (1990) 2571–2574.
15. A. R. Yavary and P. J. Desré, *Mater. Sci. Eng.* **A134** (1991) 1315–1322.
16. H. J. Fecht, *Nature* **356** (1992) 133–135.
17. A. M. Tonejc, D. Bagović, and M. Tudja, *Mater. Lett.* **20** (1994) 51–61.
18. J. Eckert, L. Schulz, and K. Urban, *J. Non-Cryst. Solids* **130** (1991) 273–277.
19. S. Hovmöller, *Ultramicroscopy* **41** (1992) 121–135.
20. A. M. Tonejc, A. Tonejc, G. W. Farrants, and S. Hovmöller, *Proceedings of EUREM-11,* Vol. 2, Dublin, 1996, pp. 125–126.
21. A. M. Tonejc, A. Tonejc, G. W. Farrants, and S. Hovmöller, *Mater. Sci. Forum* **269–272** (1998) 357–362.
22. A. Sekulić, I. Furić, A. Tonejc, A. M. Tonejc, and M. Stubičar, *J. Mater. Sci. Lett.* **16** (1997) 260–262.
23. J. L. Bailey, D. Lewis, Z. Librant, and L. J. Porter, *Trans. J. Br. Ceram. Soc.* **71** (1991) 25–30.
24. K. Kranjc, *Am. J. Phys.* **30** (1962) 342–347.
25. R. D. Heidenreich, *Fundamentals of Transmission Electron Microscopy*, Interscience Publishers, New York, 1964, p. 138.
26. X. D. Zou, Ph.D. Thesis, Stockholm University, 1995.

SAŽETAK

Objašnjenje mehaničkog legiranja smjese ZrO_2 i Y_2O_3 s pomoću računalne analize elektronsko-mikroskopskih slika visokog razlučivanja

Anđelka Tonejc, Antun Tonejc, George W. Farrants i Sven Hovmöller

Računalnom analizom elektronsko-mikroskopskih slika visokog razlučivanja ispitivali smo početak procesa mehaničkog legiranja smjese praha $ZrO_2 + Y_2O_3$ ($x = 0{,}1$). Posebnu pažnju posvetili smo područjima oko granice zrna kao i mjestima gdje su se prekrivali slojevi cirkonijeva i itrijeva oksida. Metoda Fourierova filtriranja omogućila je, da se pokaže i dokaže, na nivou atomskih razmaka, kako se legiranje zbiva u granicama zrna, te u tankim slojevima cirkonijeva i itrijeva oksida koji se prekrivaju.